

Article

Twist–Bend Nematic Phase Behavior of Cyanobiphenyl-Based Dimers with Propane, Ethoxy, and Ethylthio Spacers

Yuki Arakawa ^{*}, Yuto Arai, Kyohei Horita, Kenta Komatsu and Hideto Tsuji 

Department of Applied Chemistry and Life Science, Graduate School of Engineering, Toyohashi University of Technology, 1-1 Hibarigaoka, Tempaku-cho, Toyohashi 441-8580, Japan

^{*} Correspondence: arakawa@tut.jp

Abstract: The twist–bend nematic (N_{TB}) phase is a liquid crystal (LC) phase with a heliconical structure that typically forms below the temperature of the conventional nematic (N) phase. By contrast, the direct transition between the N_{TB} and isotropic (Iso) phases without the intermediation of the N phase rarely occurs. Herein, we demonstrate the effects of linkage type (i.e., methylene, ether, and thioether) on the typical Iso–N– N_{TB} and rare direct Iso– N_{TB} phase-transition behaviors of cyanobiphenyl (CB) dimers CB3CB, CB2OCB, and CB2SCB bearing three-atom-based propane, ethoxy, and ethylthio spacers, respectively. In our previous study, CB2SCB exhibited the monotropic direct Iso– N_{TB} phase transition. In this study, we report that CB3CB also shows the direct Iso– N_{TB} phase transition, whereas CB2OCB exhibits the typical Iso–N– N_{TB} phase sequence with decreasing temperature. The Iso–LC (Iso– N_{TB} or Iso–N) phase-transition temperatures upon cooling show the order CB2OCB (108 °C) > CB3CB (49 °C) > CB2SCB (43 °C). The thioether-linked CB2SCB is vitrifiable, whereas CB3CB and CB2OCB exhibit strong crystallization tendencies. The phase-transition behaviors are also discussed in terms of the three bent homologous series with different oligomethylene spacers n : $CBnCB$, $CBnOCB$, and $CBnSCB$.

Keywords: twist–bend nematic phase; direct twist–bend nematic phase transition; liquid crystal dimer; cyanobiphenyl dimer; short spacer



Citation: Arakawa, Y.; Arai, Y.; Horita, K.; Komatsu, K.; Tsuji, H. Twist–Bend Nematic Phase Behavior of Cyanobiphenyl-Based Dimers with Propane, Ethoxy, and Ethylthio Spacers. *Crystals* **2022**, *12*, 1734. <https://doi.org/10.3390/cryst12121734>

Academic Editors: Shigeyuki Yamada, Kyosuke Isoda, Takahiro Ichikawa, Kosuke Kaneko, Mizuho Kondo, Tsuneaki Sakurai, Atsushi Seki, Mitsuo Hara and Go Watanabe

Received: 26 October 2022

Accepted: 20 November 2022

Published: 1 December 2022

Publisher’s Note: MDPI stays neutral with regard to jurisdictional claims in published maps and institutional affiliations.



Copyright: © 2022 by the authors. Licensee MDPI, Basel, Switzerland. This article is an open access article distributed under the terms and conditions of the Creative Commons Attribution (CC BY) license (<https://creativecommons.org/licenses/by/4.0/>).

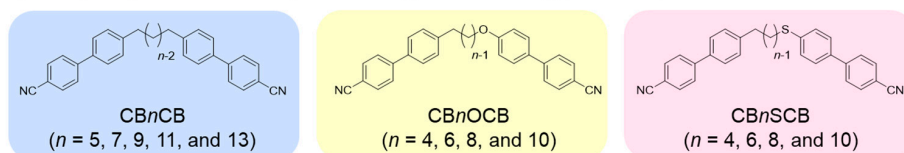
1. Introduction

Liquid crystal (LC) phases are mesophases between anisotropic crystals and isotropic liquids. A nematic (N) phase generally does not have an apparent layered structure and is recognized as the most fluid LC phase. After the heliconical twist–bend nematic (N_{TB}) phase was predicted [1–3], it was experimentally assigned to unknown N (N_X) phases below the conventional N phase of bent molecules (dimers) in the last decade [4,5]. The N_{TB} phase possesses a heliconical director precession with a pitch of approximately 10 nm [6–8]. The heliconical structures of the N_{TB} phase result in optical textures and physical properties like those of layered smectic (Sm) phases rather than the conventional N phase [9–13]. Therefore, the N_{TB} phase is often considered a pseudo-layered phase. However, the phase identification of the N_{TB} phase for the N_X phase is still under discussion and further study is required to elucidate the detailed structure owing to its elusive nature. Alternatively, a polar twisted nematic (N_{PT}) phase model for the N_X phase instead of the N_{TB} phase has been proposed [14,15]. In this paper, the widely recognized term, N_{TB} phase, is used.

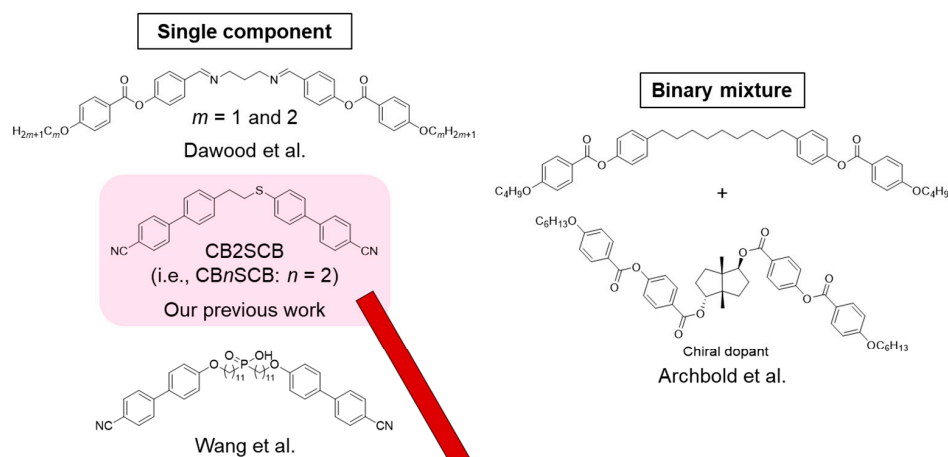
The N_{TB} phase can be formed only by bent molecules, such as bent dimers [4,5,16–39], linear oligomers (e.g., trimers, tetramers, and hexamers) [40–49], duplexed hexamers [50], polymers [51], hydrogen-bonded dimers and trimers [52,53] with odd-number atom spacers, and bent-core molecules [54–56]. Mandle reviewed the structure–property relationship of the N_{TB} phase and summarized the recent progress in this topic [57]. Theoretical simulation studies have examined the relationship between the curvature of various bent dimers and the incidence of the N_{TB} phase [58–61]. In nearly all cases of the reported bent

molecules, the N_{TB} phase continuously formed at a temperature below the temperature of the conventional N phase, resulting in a typical isotropic (Iso)–N– N_{TB} phase sequence with decreasing temperature. For example, the homologous series of bent symmetric methylene- and asymmetric methylene-/ether- and methylene-/thioether-linked cyanobiphenyl (CB) dimers with n number of carbon atoms in the oligomethylene spacers, CB_nCB ($n = 5, 7, 9, 11,$ and 13) [17,25], CB_nOCB ($n = 4, 6, 8,$ and 10) [24,25], and CB_nSCB ($n = 4, 6, 8,$ and 10) [62], respectively, are known to exhibit the typical Iso–N– N_{TB} phase sequence (Figure 1a).

(a) Cyanobiphenyl dimer homologs with the typical Iso–N– N_{TB} phase sequence



(b) Dimer systems with the rare Iso– N_{TB} phase sequence



(c) The present study

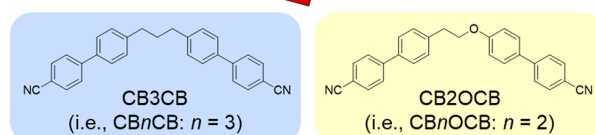


Figure 1. Bent dimer systems exhibiting the typical Iso–N– N_{TB} and rare direct Iso– N_{TB} phase transitions investigated in previous studies and the present study. (a) Previous work on bent-shaped CB dimer homologs with longer spacers, including methylene-linked CB_nCB (odd $n = 5, 7, 9, 11,$ and 13) [17,25], methylene-/ether-linked CB_nOCB (even $n = 4, 6, 8,$ and 10) [24,25], and methylene-/thioether-linked CB_nSCB ($n = 4, 6, 8,$ and 10) [62] that exhibit the typical Iso–N– N_{TB} phase sequence. (b) Previous work on dimers showing the rare Iso– N_{TB} phase sequence from binary mixtures reported by Archbold et al. [63] (right) and single-component dimers reported by Dawood et al. [64,65] (imine-linked dimers, top left), our group [62] (ethylthio-linked **CB₂SCB**, center left), and Wang et al. [66] (a phosphine-bridged dimer, bottom left). (c) Single-component dimers **CB₃CB** and **CB₂OCB** in the present study.

However, in a few cases, an N_{TB} phase can be directly formed from the Iso phase without the intermediate N phase. Archbold et al. reported that binary mixtures of a dimer with the Iso–N– N_{TB} phase sequence and a chiral dopant (6–10 wt%) exhibit the direct Iso– N_{TB} phase transition (Figure 1b, right) [63]. Dawood et al. reported that two imine-linked dimers with a central propane spacer and terminal methoxy or ethoxy groups ($m = 1$ and 2 , respectively) (Figure 1b, top left) show the direct Iso– N_{TB} phase transition [64,65]. We reported that bent CB_nSCB ($n = 4, 6, 8,$ and 10) demonstrates the Iso–N– N_{TB} phase sequence, as described earlier, whereas only the shortest ethylthio-linked **CB₂SCB** exhibits the direct Iso– N_{TB} phase transition upon cooling (Figure 1b, center left) [62]. Shortening the flexible

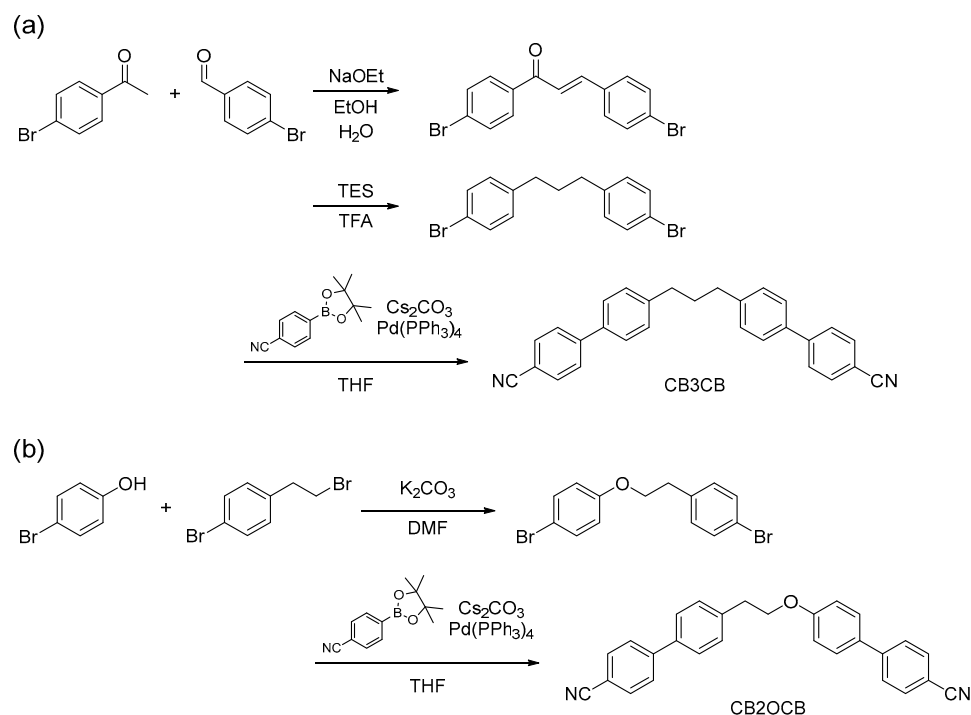
spacer n of the CB_nSCB dimers lowers the Iso–N phase-transition temperature (T_{IN}) upon cooling, thereby narrowing the intermediate N-phase temperature range (ΔT_N), which leads to the direct Iso– N_{TB} phase transition of CB_2SCB . Moreover, Wang et al. recently disclosed that a phosphorus-bridged LC dimer exhibits the direct Iso– N_{TB} phase transition (Figure 1b, bottom left) [66].

Considering that, in our previous study, CB_2SCB demonstrated the rare direct Iso– N_{TB} phase transition [62], propane-linked CB_3CB and ethoxy-linked CB_2OCB bearing the same three-atom-based spacers (as shown in Figure 1c) are worthy of further investigation whether they exhibit the rare Iso– N_{TB} phase or not. The influence of the different linkage types on the phase transition of such short-spacer dimers has yet to be reported. In this study, we investigated the phase-transition behaviors of three CB-based dimers with different three-atom-based spacers, namely CB_3CB , CB_2OCB , and CB_2SCB . The phase-transition behavior of the previously reported CB_3CB that did not show the LC phase [67] was re-investigated, while that of CB_2OCB was explored for the first time. The phase-transition data of CB_2SCB were obtained from our previous study [62]. We then compared the phase-transition behaviors of three series of CB_nCB , CB_nOCB , and CB_nSCB homologs. Finally, the effects of linkage-type on the N_{TB} phase-transition behavior of dimers with short spacers, particularly on the occurrence of the direct Iso– N_{TB} phase transition, were explored.

2. Materials and Methods

2.1. General

The synthetic routes of CB_3CB and CB_2OCB are shown in Scheme 1. The molecular structures were analyzed using 1H and ^{13}C nuclear magnetic resonance (NMR) spectroscopy on a JNM ECX 500 spectrometer (JEOL Ltd., Tokyo, Japan). Phase identification was conducted via polarized optical microscopy (POM) using a BX50 microscope (Olympus Corp., Tokyo, Japan) on an LK-600 PM hot stage (Linkam, Surrey, UK). The phase-transition temperatures and associated enthalpy changes were determined using differential scanning calorimetry (DSC) on a DSC-60 Plus (Shimadzu Corp., Kyoto, Japan). Calibration was performed using indium, and the measurements were performed over heating/cooling/heating cycles at a rate of $10\text{ }^\circ\text{C min}^{-1}$ under an N_2 gas flow (50 mL min^{-1}).



Scheme 1. Synthesis of (a) CB_3CB and (b) CB_2OCB .

2.2. Synthesis

2.2.1. 1,3-Bis(4-cyanobiphenyl-4'-yl)propane (CB3CB)

(E)-1,3-Bis(4-bromophenyl)prop-2-en-1-one

This compound was synthesized referring to a previously reported method [68]. 4'-Bromoacetophenone (2.19 g, 11.0 mmol), *p*-bromobenzaldehyde (2.04 g, 11.0 mmol), sodium ethoxide (NaOEt) (1.12 g, 16.5 mmol), ethanol (EtOH) (30 mL), and distilled water (10 mL) were added to a round-bottom flask. The resultant mixture was stirred at ambient temperature for 1 h. The reaction mixture was filtered, and the residue was rinsed with copious amounts of methanol to afford the target compound as a pale-yellow solid (86%). ¹H NMR (500 MHz, CDCl₃) δ 7.89 (d, *J* = 9.0 Hz, Ar-*H*, 2H), 7.75 (d, *J* = 16.0 Hz, CO-CH, 1H), 7.65 (d, *J* = 9.0 Hz, Ar-*H*, 2H), 7.56 (d, *J* = 9.0 Hz, Ar-*H*, 2H), 7.51 (d, *J* = 9.0 Hz, Ar-*H*, 2H), 7.47 (d, *J* = 16.0 Hz, CO-CH=CH, 1H) ppm. ¹³C NMR (126 MHz, CDCl₃) δ 189.1, 143.9, 136.7, 133.7, 132.3, 132.0, 130.0, 129.8, 128.1, 125.1, 121.9 ppm.

1,3-Bis(4-bromophenyl)propane

This compound was also synthesized referring to the literature [68]. (E)-1,3-Bis(4-bromophenyl)prop-2-en-1-one (1.10 g, 2.99 mmol) was added to a two-necked round-bottom flask, which was then purged with argon gas. Trifluoroacetic acid (TFA) (11 mL) was then added into the flask, followed by adding triethylsilane (TES) (4.8 mL, 30 mmol) dropwise. The resultant mixture was stirred at ambient temperature for 1 h. TES (0.95 mL, 5.94 mmol) was added to the reaction mixture, which was further stirred for 18 h. The reaction mixture was poured into distilled water, extracted with dichloromethane, and washed with brine. The obtained solution was then dried over magnesium sulfate (MgSO₄), and the solvent was removed under reduced pressure. The residue was purified by column chromatography on silica gel using hexane as an eluent to afford 1,3-bis(4-bromophenyl)propane as a colorless solid (78%). ¹H NMR (500 MHz, CDCl₃) δ 7.39 (d, *J* = 8.5 Hz, Ar-*H*, 4H), 7.04 (d, *J* = 8.5 Hz, Ar-*H*, 4H), 2.58 (t, *J* = 7.5 Hz, Ar-CH₂, 4H), 1.90 (tt, *J* = 7.5 and 7.5 Hz, Ar-CH₂-CH₂, 2H) ppm. ¹³C NMR (126 MHz, CDCl₃) δ 140.9, 131.4, 130.2, 119.5, 34.6, 32.6 ppm.

CB3CB

1,3-Bis(4-bromophenyl)propane (200 mg, 0.565 mmol), 4-(4,4,5,5-tetramethyl-1,3,2-dioxaborolan-2-yl)benzotrile (267 mg, 1.17 mmol), cesium carbonate (Cs₂CO₃) (748 mg, 2.29 mmol), and tetrakis(triphenylphosphine)palladium(0) [Pd(PPh₃)₄] (41.5 mg, 35.9 μmol) were added to a two-necked round-bottom flask, which was then purged with argon gas. Tetrahydrofuran (THF) (5 mL) was degassed by bubbling with argon gas and added to the flask. The resultant mixture was stirred at reflux temperature for 3 h. Subsequently, Pd(PPh₃)₄ (39.5 mg, 34.2 μmol) was added to the reaction mixture, which was further stirred for 4 h. The reaction mixture was extracted with dichloromethane and washed with brine. The solution was then dried over MgSO₄, and the volatile solvent was removed under reduced pressure. The residue was purified by column chromatography on silica gel using dichloromethane/hexane (1:1, *v/v*) and recrystallized in a dichloromethane/hexane mixture to afford CB3CB as a colorless solid (51%). ¹H NMR (500 MHz, CDCl₃) δ 7.71 (d, *J* = 8.5 Hz, Ar-*H*, 4H), 7.67 (d, *J* = 8.5 Hz, Ar-*H*, 4H), 7.53 (d, *J* = 8.5 Hz, Ar-*H*, 4H), 7.31 (d, *J* = 8.5 Hz, Ar-*H*, 4H), 2.74 (t, *J* = 7.5 Hz, Ar-CH₂, 4H), 2.04 (tt, *J* = 7.5 and 7.5 Hz, Ar-CH₂-CH₂, 2H) ppm. ¹³C NMR (126 MHz, CDCl₃) δ 145.5, 142.9, 136.7, 132.6, 129.2, 127.5, 127.2, 119.0, 110.6, 35.0, 32.7 ppm.

2.2.2. (4-Cyanobiphenyl-4'-yloxy)-2-(4-cyanobiphenyl-4'-yl)ethane (CB2OCB)

1-Bromo-4-[2-(4-bromophenoxy)ethyl]benzene

4-Bromophenethyl bromide (690 mg, 2.61 mmol), 4-bromophenol (302 mg, 1.75 mmol), and potassium carbonate (K₂CO₃) (617 mg, 4.46 mmol) were added to a two-necked round-bottom flask, which was then purged with argon gas. *N,N*-Dimethylformamide (DMF) (5 mL) was degassed by bubbling argon gas and then added to the flask. The resultant

mixture was stirred at 90 °C for 18 h. More 4-bromophenethyl bromide (690 mg, 2.61 mmol) was added to the reaction mixture, which was further stirred for 5 h. The reaction mixture was extracted with ethyl acetate and washed with brine. The obtained solution was dried over MgSO₄, and then the solvent was removed under reduced pressure. The residue was purified by column chromatography on silica gel using hexane/ethyl acetate (20:1, *v/v*) to afford 1-Bromo-4-[2-(4-bromophenoxy)ethyl]benzene (28%). ¹H NMR (500 MHz, CDCl₃) δ 7.43 (d, *J* = 8.5 Hz, Ar-*H*, 2H), 7.35 (d, *J* = 8.5 Hz, Ar-*H*, 2H), 7.14 (d, *J* = 8.5 Hz, Ar-*H*, 2H), 6.75 (d, *J* = 8.5 Hz, Ar-*H*, 2H), 4.11 (t, *J* = 6.5 Hz, Ar-O-CH₂, 2H), 3.03 (t, *J* = 6.8 Hz, Ar-O-CH₂-CH₂, 2H) ppm. ¹³C NMR (126 MHz, CDCl₃) δ 157.8, 137.1, 132.3, 131.6, 130.7, 120.4, 116.3, 113.0, 68.5, 35.1 ppm.

CB2OCB

1-Bromo-4-[2-(4-bromophenoxy)ethyl]benzene (96.7 mg, 0.272 mmol), 4-(4,4,5,5-tetramethyl-1,3,2-dioxaborolan-2-yl)benzotrile (140 mg, 0.611 mmol), Cs₂CO₃ (182 mg, 0.559 mmol), and Pd(PPh₃)₄ (64.1 mg, 55.5 μmol) were added to a two-necked round-bottom flask, which was then purged with argon gas. THF (3 mL) was degassed by bubbling argon gas and then added to the flask. The resultant mixture was stirred at reflux temperature for 16 h. An arbitrary amount of Pd(PPh₃)₄ was added to the reaction mixture. The mixture was then stirred for 16 h, extracted with dichloromethane, and washed with brine. The solution was dried over MgSO₄, and the volatile solvent was removed under reduced pressure. The residue was purified by column chromatography on silica gel using dichloromethane/hexane (5:1, *v/v*) and recrystallized in a dichloromethane/hexane mixture to afford CB2OCB (20%). ¹H NMR (500 MHz, CDCl₃) δ 7.72 (d, *J* = 8.5 Hz, Ar-*H*, 2H), 7.69 (d, *J* = 8.5 Hz, Ar-*H*, 2H), 7.67 (d, *J* = 8.0 Hz, Ar-*H*, 2H), 7.63 (d, *J* = 8.5 Hz, Ar-*H*, 2H), 7.55 (d, *J* = 8.5 Hz, Ar-*H*, 2H), 7.52 (d, *J* = 9.0 Hz, Ar-*H*, 2H), 7.42 (d, *J* = 8.0 Hz, Ar-*H*, 2H), 7.00 (d, *J* = 9.0 Hz, Ar-*H*, 2H), 4.27 (t, *J* = 6.5 Hz, Ar-O-CH₂, 2H), 3.18 (t, *J* = 6.5 Hz, Ar-O-CH₂-CH₂, 2H) ppm. ¹³C NMR (126 MHz, CDCl₃) δ 159.3, 145.3, 145.1, 138.9, 137.5, 132.59, 132.56, 131.7, 129.8, 128.4, 127.5, 127.3, 127.1, 119.1, 118.9, 115.1, 110.8, 110.1, 68.5, 35.3 ppm.

3. Results

3.1. Phase-Transition Behaviors of CB3CB, CB2OCB, and CB2SCB

As shown in the DSC curves (Figure 2a), the methylene-linked CB3CB sample exhibited a melting temperature (*T*_m) of ~149 °C, where it transitioned to the Iso phase without forming the LC phase upon heating. Upon cooling, the CB3CB sample crystallized at ~80 °C from the Iso phase. These phase-transition temperatures were higher than those (142.1 and 69.1 °C, respectively) reported in the literature [67], where CB3CB did not exhibit the LC phase. However, POM observations in this study revealed that in the supercooled Iso phase of CB3CB (Figure 3a), which does not undergo crystallization at ~80 °C, birefringent textures appear (Figure 3b), which then grow mixed textures including fan-, focal-conic-, and rope-like domains, as shown in Figure 3c,d. Besides, we did not observe typical N-phase textures such as marble and schlieren textures during this phase transition, as seen in Figure 3. This texture behavior is similar to the direct Iso-N_{TB} phase transition of CB2SCB [62]. Therefore, it was revealed that CB3CB also shows the monotropic direct Iso-N_{TB} phase transition at ~49 °C. During the heating after the cooling, the observed N_{TB} phase of CB3CB transitioned to the Iso phase at ~55 °C. The CB3CB sample displayed a strong crystallization tendency and did not vitrify upon cooling, even at a higher rate of 30 °C min⁻¹. Additionally, the ether-linked CB2OCB did not show LC phases over the first and second heating cycles, where it exhibited different *T*_m values of 164.4 and 139.7 °C, respectively; Figure 2b represents the latter. This result indicates the existence of crystal polymorphs that depend on the crystallization conditions. Upon cooling, most of the Iso-phase domains and droplets of CB2OCB crystallize at ~104 °C, as shown by the exothermic peak in Figure 2b. However, the POM images reveal the formation of the N and N_{TB} phases at ~108 and 78 °C, respectively, in the supercooled Iso phase, as confirmed

by the marble/schlieren textures (Figure 4a) and blocky texture (Figure 4b), respectively. Because of the strong crystallization tendencies of CB3CB and CB2OCB, as shown by the DSC curves (Figure 2a,b, respectively), their LC phases were not investigated by X-ray diffractometry. The strong crystallization tendency of these molecules differs from the vitrifiable CB2SCB, with a glass transition temperature of ~ 20 °C, as shown in Figure 2c [62]. The T_m values upon the second heating, the associated enthalpy changes (ΔH), and the Iso- N_{TB} , Iso-N, and N- N_{TB} phase-transition temperatures upon the cooling (T_{INTB} , T_{IN} , and T_{NNTB} , respectively) of CB3CB, CB2OCB, and CB2SCB are summarized in Table 1. For simplicity, the crystallization and glass transition temperatures upon cooling are not listed in Table 1.

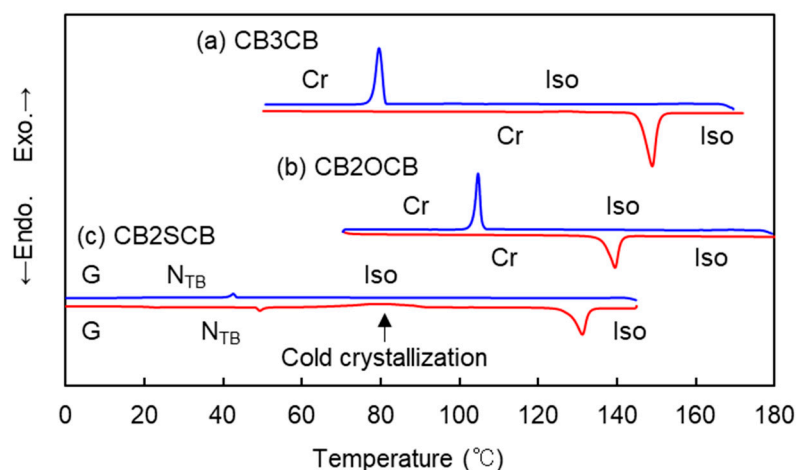


Figure 2. DSC curves of (a) CB3CB, (b) CB2OCB, and (c) CB2SCB upon the second heating (red lines) and cooling (blue lines) cycles at a rate of 10 °C min^{-1} . Cr and G denote the crystal phase and glassy state, respectively. Panel (c) is reproduced from Ref. [62].

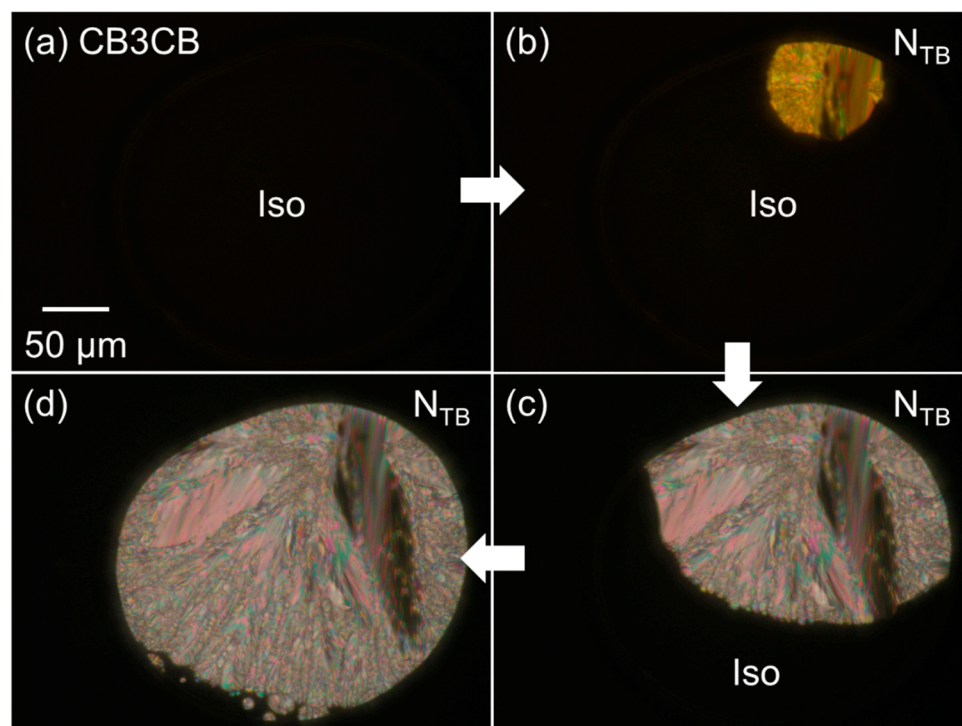


Figure 3. POM images during the Iso- N_{TB} phase transition of CB3CB: (a) the Iso phase (52 °C), (b) the N_{TB} texture appearance in the Iso phase (50 °C), (c,d) growth in the N_{TB} texture (48.5 and 47.5 °C, respectively).

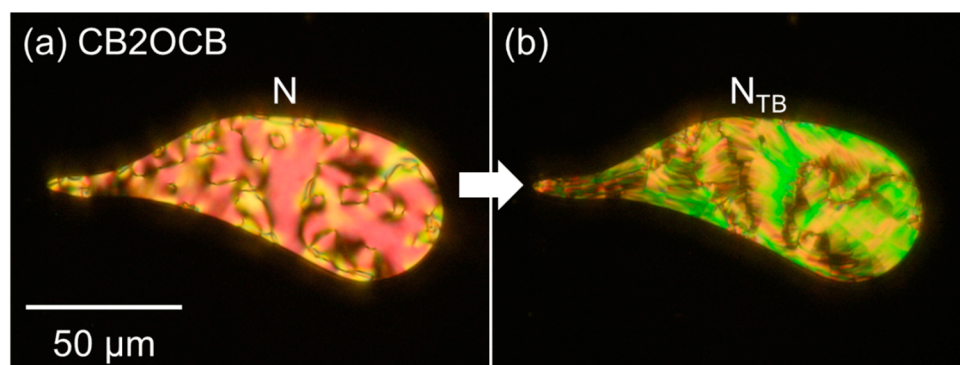


Figure 4. POM images of (a) the N phase (104 °C) and (b) the N_{TB} phase (69 °C) of CB2OCB.

Table 1. T_m and the associated ΔH upon second heating and T_{INTB} , T_{IN} , and T_{NNTB} upon cooling for CB3CB, CB2OCB, and CB2SCB.

Sample	Heating	Cooling
CB3CB	$T_m = 149.0\text{ °C}$ ($\Delta H = 30.9\text{ kJ mol}^{-1}$)	$T_{INTB} = 49\text{ °C}$ ^a
CB2OCB	$T_m = 139.7\text{ °C}$ ($\Delta H = 25.5\text{ kJ mol}^{-1}$)	$T_{IN} = 108\text{ °C}$ ^a , $T_{NNTB} = 78\text{ °C}$ ^a
CB2SCB	$T_m = 131.0\text{ °C}$ ($\Delta H = 24.4\text{ kJ mol}^{-1}$) ^{b,c}	$T_{INTB} = 42.6\text{ °C}$ ^b

^a Determined by POM. ^b Obtained from Ref. [62]. ^c Obtained upon first heating.

Thus, CB3CB and CB2SCB exhibited the direct Iso- N_{TB} phase transition, whereas CB2OCB showed the typical Iso-N- N_{TB} phase transition. Moreover, the CB3CB and CB2OCB samples displayed a stronger crystallization tendency compared with the thioether-linked CB2SCB, which had a vitrifiable N_{TB} phase [62]. The Iso-LC phase-transition temperatures (i.e., T_{INTB} or T_{IN}) showed the order CB2OCB (108 °C) \gg CB3CB (49 °C) $>$ CB2SCB (43 °C), which translated to the order ether \gg methylene $>$ thioether in terms of linkage type. Naturally, the N_{TB} phase-transition temperatures (i.e., T_{INTB} or T_{NNTB}) also showed the same order: ether \gg methylene $>$ thioether. This particularly high phase-transition temperature (especially for the LC-Iso or Iso-LC phase transition) with the ether linkage is typical for usual calamitic LCs [69–71], including bent LC dimers [28,30,31,33,37,39]. Additionally, CB2SCB is vitrifiable, whereas CB3CB and CB2OCB strongly crystallize. These trends in the LC phase-transition temperatures and crystallization or vitrification abilities of the three dimers could be attributed to their different linkages, that is, ether (C–O–C), methylene (C–CH₂–C), and thioether (C–S–C). The C–O–C bond angle (118°) is larger than those of the other linkage types, which renders CB2OCB more anisotropic [72]. In addition, The higher rotational barrier [73,74] and stronger electron-donating property of the Ph–O bond may contribute to the molecular rigidity and intermolecular interactions of CB2OCB, respectively. These could result in higher T_{IN} and T_{NNTB} , a larger ΔT_N , and, possibly, at least in part, a stronger crystallization tendency. The higher T_{INTB} of CB3CB compared with that of CB2SCB is attributed to its higher molecular anisotropy owing to the larger C–CH₂–C bond angle (~110°) compared with the C–S–C angle (~100°), as well as higher rigidity due to the higher rotational barrier of the C–CH₂ bond compared with that of the C–S bond [75]. The higher T_m and T_{IN} and stronger crystallization tendency of CB3CB compared with those of CB2SCB could also be attributed to the symmetric molecular structure of the former. A more bent, flexible C–S–C linkage and molecular asymmetry endow CB2SCB with lower phase-transition temperatures and a vitrification ability compared with CB3CB and CB2OCB [33,39,62].

3.2. Phase-Transition Behaviors of CB n CB, CB n OCB, and CB n SCB

As described in the Introduction, each bent CB-based dimer homolog series with the longer spacers CB n CB ($n = 5, 7, 9, 11,$ and 13) [17,25], CB n OCB ($n = 4, 6, 8,$ and 10) [24,25], and CB n SCB ($n = 4, 6, 8,$ and 10) [62] exhibit the typical Iso-N- N_{TB} phase sequence. The

T_{IN} , T_{NNTB} , and ΔT_N of these homologous series are plotted in Figure 5a–c, respectively, as a function of the total number of atoms in the spacer chain lengths, i.e., n for $CBnCB$ and $n + 1$ for $CBnOCB$ and $CBnSCB$, including the O and S atoms. The T_{INTB} values of $CB3CB$ and $CB2SCB$ are included in the plots shown in Figure 5a,b.

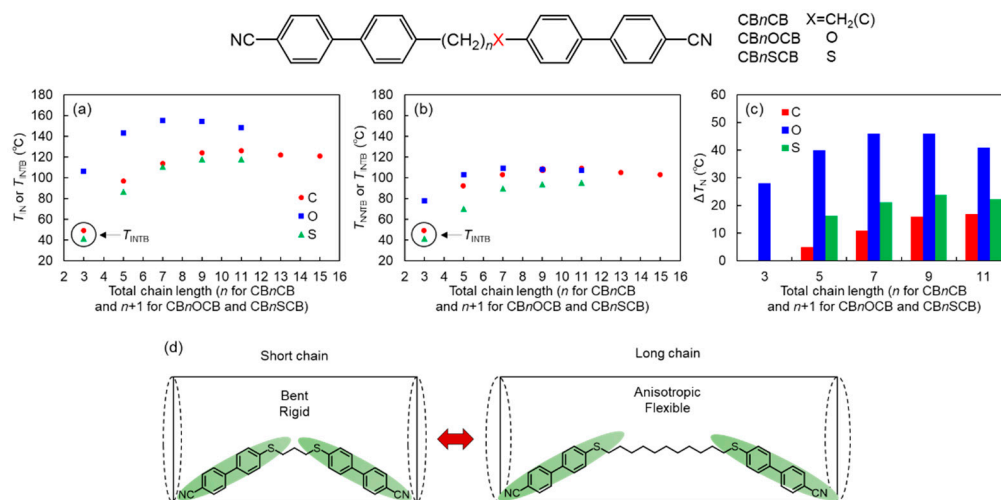


Figure 5. (a) T_{IN} , (b) T_{NNTB} , (c) ΔT_N , and (d) schematic models of dimers with shorter and longer spacers showing anisotropy and flexibility. In (a,b), the T_{INTB} values are plotted for $CB3CB$ and $CB2SCB$ because they exhibit the Iso- N_{TB} phase transition. Panel (d) was reproduced from Ref. [39].

Overall, the T_{IN} and T_{NNTB} values were approximately in the order of $CBnOCB > CBnCB > CBnSCB$, which could be similarly ascribed to the characteristics of the linkers described in Section 3.1 for the shortest homologs. Nevertheless, the T_{NNTB} values of the ether-linked $CBnOCB$ were relatively close to or partly lower than those of the methylene-linked $CBnCB$. This observation may partly be attributed to the characteristics of the more anisotropic structure of $CBnOCB$ because the N_{TB} phase formation for a more anisotropic molecular structure likely requires greater supercooling of the N phase compared to a more bent one [33]. Consequently, the ΔT_N values are in the order of $CBnOCB > CBnSCB > CBnCB$ for all n , as shown in Figure 5c. The ΔT_N values of the ether-linked $CBnOCB$ homologs are significantly larger than those of the others for all n owing to their high T_{IN} values.

Next, we investigated the n dependence of the phase-transition temperatures of the three homologs. The T_{IN} (or T_{INTB}) and T_{NNTB} values for all the $CBnCB$, $CBnOCB$, and $CBnSCB$ homologs increase with increasing n and then level off or gradually decline with a further increase in n , as shown in Figure 5a,b. Consequently, with increasing n , ΔT_N increases for all the homologs, reaches a maximum, and then gradually declines for $CBnCB$ and $CBnOCB$, as shown in Figure 5c. These trends of T_{IN} (or T_{INTB}), T_{NNTB} , and ΔT_N for all the dimer homologs could be attributed to the average molecular shape and flexibility with increasing/decreasing n , as shown in Figure 5d [39]. The shortest dimers could be more bent (strong biaxiality); hence, their T_{IN} (or T_{INTB}) and T_{NNTB} values were lower than those of the longer dimers. With increasing n , the average molecular shape of the bent dimer homologs becomes more linear (or anisotropic), thereby increasing T_{IN} and T_{NNTB} to some extent. However, further lengthening of the central spacer could enhance the molecular flexibility and dilute the polarizable mesogenic arms that increase the phase-transition temperatures; hence, these phase-transition temperatures nearly remain constant or gradually decline. Thus, the molecular biaxiality (molecular curvature) of the dimer homologs increases with decreasing n , which principally decreases T_{IN} , and consequently, ΔT_N . This results in $\Delta T_N = 0$, i.e., the direct Iso- N_{TB} phase transition for the shortest $CB3CB$ and $CB2SCB$ [62].

4. Conclusions

In this study, we evaluated the phase-transition behaviors of three CB-based dimers with propane, ethoxy, and ethylthio spacers. Analogous to the previously reported CB2SCB, the short CB3CB exhibited the rare direct Iso–N_{TB} phase transition, whereas CB2OCB showed the typical Iso–N–N_{TB} phase transition. CB3CB and CB2OCB have strong crystallization tendencies, whereas the thioether-linked CB2SCB exhibited a vitrifiable N_{TB} phase. The N_{TB} phase-transition temperature (T_{INTB} or T_{NNTB}) decreased in the order CB2OCB (76 °C) > CB3CB (49 °C) > CB2SCB (43 °C). The phase-transition behaviors of all the CB_nCB, CB_nOCB, and CB_nSCB homologs, including those with longer chains, were comprehensively examined. The more anisotropic ether-linked CB_nOCB series showed significantly higher T_{IN} and wider ΔT_N for all n . Regarding shorter spacers, the phase-transition temperatures decreased, especially T_{IN} . Hence, the ΔT_N for all three homologous series decreased, resulting in the direct Iso–N_{TB} phase transition for the short-spacer-bearing CB3CB and CB2SCB. This phenomenon could partly be ascribed to their bent molecular geometry or enhanced molecular biaxiality owing to their short lengths. Our findings provide new insights into the effects of linkage types on the molecular design of LC dimers that exhibit the direct Iso–N_{TB} phase transition.

Author Contributions: Conceptualization, Y.A. (Yuki Arakawa); methodology, Y.A. (Yuki Arakawa); validation, Y.A. (Yuki Arakawa); formal analysis, Y.A. (Yuki Arakawa), Y.A. (Yuto Arai), K.H., and K.K.; investigation, Y.A. (Yuki Arakawa), Y.A. (Yuto Arai), K.H., and K.K.; resources, Y.A. (Yuki Arakawa) and H.T.; data curation, Y.A. (Yuki Arakawa); writing—original draft preparation, Y.A. (Yuki Arakawa); writing—review and editing, Y.A. (Yuki Arakawa), Y.A. (Yuto Arai), K.H., and H.T.; supervision, Y.A. (Yuki Arakawa) and H.T.; project administration, Y.A. (Yuki Arakawa); funding acquisition, Y.A. (Yuki Arakawa). All authors have read and agreed to the published version of the manuscript.

Funding: This research was funded by the Japan Society for the Promotion of Science (KAKENHI grant numbers 17K14493 and 20K15351) and Toyohashi University of Technology.

Data Availability Statement: Data are presented in the article.

Conflicts of Interest: The authors declare no financial conflict of interest.

References

1. Meyer, R.B. Structural Problems in Liquid Crystal Physics. In *Molecular Fluids: Summer School in Theoretical Physics, Les Houches Lectures 1973*; Balian, R., Weil, G., Eds.; Gordon and Breach: New York, NY, USA, 1976; pp. 271–343.
2. Dozov, I. On the spontaneous symmetry breaking in the mesophases of achiral banana-shaped molecules. *Europhys. Lett.* **2011**, *56*, 247–253. [[CrossRef](#)]
3. Memmer, R. Liquid crystal phases of achiral banana-shaped molecules: A computer simulation study. *Liq. Cryst.* **2002**, *29*, 483–496. [[CrossRef](#)]
4. Cestari, M.; Diez-Berart, S.; Dunmur, D.A.; Ferrarini, A.; de la Fuente, M.R.; Jackson, D.J.B.; Lopez, D.O.; Luckhurst, G.R.; Perez-Jubindo, M.A.; Richardson, R.M.; et al. Phase behavior and properties of the liquid-crystal dimer 1',7''-bis(4-cyanobiphenyl-4'-yl) heptane: A twist-bend nematic liquid crystal. *Phys. Rev. E* **2011**, *84*, 31704. [[CrossRef](#)]
5. Panov, V.P.; Nagaraj, M.; Vij, J.K.; Panarin, Y.P.; Kohlmeier, A.; Tamba, M.G.; Lewis, R.A.; Mehl, G.H. Spontaneous periodic deformations in nonchiral planar-aligned bimesogens with a nematic-nematic transition and a negative elastic constant. *Phys. Rev. Lett.* **2010**, *105*, 167801. [[CrossRef](#)] [[PubMed](#)]
6. Chen, D.; Porada, J.H.; Hooper, J.B.; Klitnick, A.; Shen, Y.; Tuchband, M.R.; Korblova, E.; Bedrov, D.; Walba, D.M.; Glaser, M.A.; et al. Chiral helical ground state of nanoscale pitch in a nematic liquid crystal of achiral molecular dimers. *Proc. Natl. Acad. Sci. USA* **2013**, *110*, 15931–15936. [[CrossRef](#)]
7. Borshch, V.; Kim, Y.-K.; Xiang, J.; Gao, M.; Jáklí, A.; Panov, V.P.; Vij, J.K.; Imrie, C.T.; Tamba, M.G.; Mehl, G.H.; et al. Nematic twist-bend phase with nanoscale modulation of molecular orientation. *Nat. Commun.* **2013**, *4*, 2635. [[CrossRef](#)]
8. Zhu, C.; Tuchband, M.R.; Young, A.; Shuai, M.; Scarbrough, A.; Walba, D.M.; Maclennan, J.E.; Wang, C.; Hexemer, A.; Clark, N.A. Resonant carbon K-edge soft X-ray scattering from lattice-free helical molecular ordering: Soft dilative elasticity of the twist-bend liquid crystal phase. *Phys. Rev. Lett.* **2016**, *116*, 147803. [[CrossRef](#)]
9. Salili, S.M.; Kim, C.; Sprunt, S.; Gleeson, J.T.; Parri, O.; Jáklí, A. Flow properties of a twist-bend nematic liquid crystal. *RSC Adv.* **2014**, *4*, 57419–57423. [[CrossRef](#)]
10. Challa, P.K.; Borshch, V.; Parri, O.; Imrie, C.T.; Sprunt, S.N.; Gleeson, J.T.; Lavrentovich, O.D.; Jáklí, A. Twist-bend nematic liquid crystals in high magnetic fields. *Phys. Rev. E* **2014**, *89*, 060501. [[CrossRef](#)]

11. Merkel, K.; Kocot, A.; Welch, C.; Mehl, G.H. Soft modes of the dielectric response in the twist–bend nematic phase and identification of the transition to a nematic splay bend phase in the CBC7CB dimer. *Phys. Chem. Chem. Phys.* **2019**, *21*, 22839–22848. [[CrossRef](#)] [[PubMed](#)]
12. Zhou, J.; Tang, W.; Arakawa, Y.; Tsuji, H.; Aya, S. Viscoelastic properties of a thioether-based heliconical twist–bend nematogen. *Phys. Chem. Chem. Phys.* **2020**, *22*, 9593–9599. [[CrossRef](#)] [[PubMed](#)]
13. Kumar, M.P.; Kula, P.; Dhara, S. Smecticlike rheology and pseudolayer compression elastic constant of a twist–bend nematic liquid crystal. *Phys. Rev. Mater.* **2020**, *4*, 115601. [[CrossRef](#)]
14. Vanakaras, A.G.; Photinos, D.J. A molecular theory of nematic–nematic phase transitions in mesogenic dimers. *Soft Matter* **2016**, *12*, 2208–2220. [[CrossRef](#)] [[PubMed](#)]
15. Samulski, E.T.; Reyes-Arango, D.; Vanakaras, A.G.; Photinos, D.J. All Structures Great and Small: Nanoscale Modulations in Nematic Liquid Crystals. *Nanomaterials* **2021**, *12*, 93. [[CrossRef](#)] [[PubMed](#)]
16. Sepelj, M.; Baumeister, U.; Ivšić, T.; Lesac, A. Effects of geometry and electronic structure on the molecular self-assembly of naphthyl-based dimers. *J. Phys. Chem. B* **2013**, *117*, 8918–8929. [[CrossRef](#)]
17. Henderson, P.A.; Imrie, C.T. Methylene-linked liquid crystal dimers and the twist–bend nematic phase. *Liq. Cryst.* **2011**, *38*, 1407–1414. [[CrossRef](#)]
18. Sebastian, N.; Lopez, D.O.; Robles-Hernandez, B.; de la Fuente, M.R.; Salud, J.; Perez-Jubindo, M.A.; Dunmur, D.A.; Luckhurst, G.R.; Jackson, D.J.B. Dielectric, calorimetric and mesophase properties of 1''-(2',4'-difluorobiphenyl-4'-yloxy)-9''-(4-cyanobiphenyl-4'-yloxy) nonane: An odd liquid crystal dimer with a monotropic mesophase having the characteristics of a twist–bend nematic phase. *Phys. Chem. Chem. Phys.* **2014**, *16*, 21391–21406. [[CrossRef](#)]
19. Mandle, R.J.; Davis, E.J.; Archbold, C.T.; Voll, C.C.A.; Andrews, J.L.; Cowling, S.J.; Goodby, J.W. Apolar bimesogens and the incidence of the twist–bend nematic phase. *Chem. Eur. J.* **2015**, *21*, 8158–8167. [[CrossRef](#)]
20. Ahmed, Z.; Welch, C.; Mehl, G.H. The design and investigation of the selfassembly of dimers with two nematic phases. *RSC Adv.* **2015**, *5*, 93513–93521. [[CrossRef](#)]
21. Mandle, R.J.; Voll, C.C.A.; Lewis, D.J.; Goodby, J.W. Etheric bimesogens and the twist–bend nematic phase. *Liq. Cryst.* **2016**, *4*, 13–21. [[CrossRef](#)]
22. Mandle, R.J.; Goodby, J.W. Does Topology Dictate the Incidence of the Twist–Bend Phase? Insights Gained from Novel Unsymmetrical Bimesogens. *Chem. Eur. J.* **2016**, *22*, 18456–18464. [[CrossRef](#)]
23. Ivšić, T.; Vinković, M.; Baumeister, U.; Mikleušević, A.; Lesac, A. Towards understanding the N_{TB} phase: A combined experimental, computational and spectroscopic study. *RSC Adv.* **2016**, *6*, 5000–5007. [[CrossRef](#)]
24. Paterson, D.A.; Gao, M.; Kim, Y.K.; Jamali, A.; Finley, K.L.; Robles-Hernández, B.; Diez-Berart, S.; Salud, J.; de la Fuente, M.R.; Timimi, B.A.; et al. Understanding the twist–bend nematic phase: The characterisation of 1-(4-cyanobiphenyl-4'-yloxy)-6-(4-cyanobiphenyl-4'-yl)hexane (CB6OCB) and comparison with CB7CB. *Soft Matter* **2016**, *12*, 6827–6840. [[CrossRef](#)] [[PubMed](#)]
25. Paterson, D.A.; Abberley, J.P.; Harrison, W.T.A.; Storey, J.M.D.; Imrie, C.T. Cyanobiphenyl-based liquid crystal dimers and the twist–bend nematic phase. *Liq. Cryst.* **2017**, *44*, 127–146. [[CrossRef](#)]
26. Knežević, A.; Sapunar, M.; Buljan, A.; Dokli, I.; Hameršak, Z.; Kontrec, D.; Lesac, A. Fine-tuning the effect of pep interactions on the stability of the N_{TB} phase. *Soft Matter* **2018**, *14*, 8466–8474. [[CrossRef](#)] [[PubMed](#)]
27. Watanabe, K.; Tamura, T.; Kang, S.; Tokita, M. Twist bend nematic liquid crystals prepared by one-step condensation of 4-(4-Pentylcyclohexyl) benzoic acid and alkyl diol. *Liq. Cryst.* **2018**, *45*, 924–930. [[CrossRef](#)]
28. Arakawa, Y.; Komatsu, K.; Tsuji, H. Twist–bend nematic liquid crystals based on thioether linkage. *New J. Chem.* **2019**, *43*, 6786–6793. [[CrossRef](#)]
29. Zep, A.; Pruszkowska, K.; Dobrzycki, Ł.; Sektas, K.; Szałański, P.; Marek, P.H.; Cyrański, M.K.; Siciński, R.R. Cholesterol-based photo-switchable mesogenic dimers. Strongly bent molecules versus an intercalated structure. *CrystEngComm* **2019**, *21*, 2779–2789. [[CrossRef](#)]
30. Arakawa, Y.; Tsuji, H. Selenium-linked liquid crystal dimers for twist–bend nematogens. *J. Mol. Liq.* **2019**, *289*, 111097. [[CrossRef](#)]
31. Cruickshank, E.; Salamonczyk, M.; Pocięcha, D.; Strachan, G.J.; Storey, J.M.D.; Wang, C.; Feng, J.; Zhu, C.; Gorecka, E.; Imrie, C.T. Sulfur-linked cyanobiphenylbased liquid crystal dimers and the twist–bend nematic phase. *Liq. Cryst.* **2019**, *46*, 1595–1609. [[CrossRef](#)]
32. Walker, R.; Pocięcha, D.; Storey, J.M.D.; Gorecka, E.; Imrie, C.T. The Chiral Twist–Bend Nematic Phase (N^{*}_{TB}). *Chem. Eur. J.* **2019**, *25*, 13329–13335. [[CrossRef](#)] [[PubMed](#)]
33. Arakawa, Y.; Ishida, Y.; Tsuji, H. Ether-and Thioether-Linked Naphthalene-Based Liquid-Crystal Dimers: Influence of Chalcogen Linkage and Mesogenic-Arm Symmetry on the Incidence and Stability of the Twist–Bend Nematic Phase. *Chem. Eur. J.* **2020**, *26*, 3767–3775. [[CrossRef](#)] [[PubMed](#)]
34. Forsyth, E.; Paterson, D.A.; Cruickshank, E.; Strachan, G.J.; Gorecka, E.; Walker, R.; Storey, J.M.D.; Imrie, C.T. Liquid crystal dimers and the twist–bend nematic phase: On the role of spacers and terminal alkyl chains. *J. Mol. Liq.* **2020**, *320*, 114391. [[CrossRef](#)]
35. Arakawa, Y.; Komatsu, K.; Feng, J.; Zhu, C.; Tsuji, H. Distinct twist–bend nematic phase behaviors associated with the ester-linkage direction of thioether-linked liquid crystal dimers. *Mater. Adv.* **2021**, *2*, 261–272. [[CrossRef](#)]
36. Walker, R.; Majewska, M.; Pocięcha, D.; Makal, A.; Storey, J.M.D.; Gorecka, E.; Imrie, C. Twist–bend nematic glasses: The synthesis and characterisation of pyrene-based nonsymmetric dimers. *ChemPhysChem* **2021**, *22*, 461–470. [[CrossRef](#)] [[PubMed](#)]

37. Arakawa, Y.; Ishida, Y.; Komatsu, K.; Arai, Y.; Tsuji, H. Thioether-linked benzylideneaniline-based twist-bend nematic liquid crystal dimers: Insights into spacer lengths, mesogenic arm structures, and linkage types. *Tetrahedron* **2021**, *95*, 132351. [[CrossRef](#)]
38. Arakawa, Y.; Komatsu, K.; Ishida, Y.; Igawa, K.; Tsuji, H. Carbonyl-and thioether-linked cyanobiphenyl-based liquid crystal dimers exhibiting twist-bend nematic phases. *Tetrahedron* **2021**, *81*, 131870. [[CrossRef](#)]
39. Arakawa, Y. Twist-bend Nematic Liquid Crystals Bearing Chalcogen-based Linkages. *EKISHO* **2021**, *25*, 221–229.
40. Mandle, R.J.; Goodby, J.W. A liquid crystalline oligomer exhibiting nematic and twist-bend nematic mesophases. *ChemPhysChem* **2016**, *17*, 967–970. [[CrossRef](#)] [[PubMed](#)]
41. Simpson, F.P.; Mandle, R.J.; Moore, J.N.; Goodby, J.W. Investigating the Cusp between the nano-and macro-sciences in super-molecular liquid-crystalline twist-bend nematogens. *J. Mater. Chem. C* **2017**, *5*, 5102–5110. [[CrossRef](#)]
42. Tuchband, M.R.; Paterson, D.A.; Salamończyk, M.; Norman, V.A.; Scarbrough, A.N.; Forsyth, E.; Garcia, E.; Wang, C.; Storey, J.M.D.; Walba, D.M.; et al. Distinct differences in the nanoscale behaviors of the twist-bend liquid crystal phase of a flexible linear trimer and homologous dimer. *Proc. Natl. Acad. Sci. USA* **2019**, *116*, 10698–10704. [[CrossRef](#)] [[PubMed](#)]
43. Saha, R.; Babakhanova, G.; Parsouzi, Z.; Rajabi, M.; Gyawali, P.; Welch, C.; Mehl, G.H.; Gleeson, J.; Lavrentovich, O.D.; Sprunt, S.; et al. Oligomeric odd-even effect in liquid crystals. *Mater. Horiz.* **2019**, *6*, 1905–1912. [[CrossRef](#)]
44. Arakawa, Y.; Komatsu, K.; Inui, S.; Tsuji, H. Thioether-linked liquid crystal dimers and trimers: The twist-bend nematic phase. *J. Mol. Struct.* **2020**, *1199*, 126913. [[CrossRef](#)]
45. Al-Janabi, A.; Mandle, R.J. Utilising saturated hydrocarbon isosteres of para benzene in the design of twist-bend nematic liquid crystals. *ChemPhysChem* **2020**, *21*, 697–701. [[CrossRef](#)] [[PubMed](#)]
46. Arakawa, Y.; Komatsu, K.; Shiba, T.; Tsuji, H. Phase behaviors of classic liquid crystal dimers and trimers: Alternate induction of smectic and twist-bend nematic phases depending on spacer parity for liquid crystal trimers. *J. Mol. Liq.* **2021**, *326*, 115319. [[CrossRef](#)]
47. Majewska, M.M.; Forsyth, E.; Pocięcha, D.; Wang, C.; Storey, J.M.D.; Imrie, C.T.; Gorecka, E. Controlling spontaneous chirality in achiral materials: Liquid crystal oligomers and the heliconical twist-bend nematic phase. *Chem. Commun.* **2022**, *58*, 5285–5288. [[CrossRef](#)]
48. Arakawa, Y.; Komatsu, K.; Tsuji, H. 2, 7-substituted fluorenone-based liquid crystal trimers: Twist-bend nematic phase induced by outer thioether linkage. *Phase Transit.* **2022**, *95*, 331–339. [[CrossRef](#)]
49. Arakawa, Y.; Komatsu, K.; Ishida, Y.; Shiba, T.; Tsuji, H. Thioether-linked liquid crystal trimers: Odd-even effects of spacers and the influence of thioether bonds on phase behavior. *Materials* **2022**, *15*, 1709. [[CrossRef](#)]
50. Mandle, R.J.; Goodby, J.W. A Nanohelicoidal Nematic Liquid Crystal Formed by a Non-Linear Duplexed Hexamer. *Angew. Chem. Int. Ed.* **2018**, *57*, 7096–7100. [[CrossRef](#)]
51. Stevenson, W.D.; An, J.; Zeng, X.B.; Xue, M.; Zou, H.X.; Liu, Y.S.; Ungar, G. Twist-bend nematic phase in biphenylethane-based copolyethers. *Soft Matter* **2018**, *14*, 3003–3011. [[CrossRef](#)]
52. Jansze, S.M.; Martínez-Felipe, A.; Storey, J.M.D.; Marcelis, A.T.M.; Imrie, C.T. A twist-bend nematic phase driven by hydrogen bonding. *Angew. Chem. Int. Ed.* **2015**, *127*, 653–656. [[CrossRef](#)]
53. Walker, R.; Pocięcha, D.; Martínez-Felipe, A.; Storey, J.M.D.; Gorecka, E.; Imrie, C.T. Twist-bend nematogenic supramolecular dimers and trimers formed by hydrogen bonding. *Crystals* **2020**, *10*, 175. [[CrossRef](#)]
54. Chen, D.; Nakata, M.; Shao, R.; Tuchband, M.R.; Shuai, M.; Baumeister, U.; Weissflog, W.; Walba, D.M.; Glaser, M.A.; MacLennan, J.E.; et al. Twist-bend heliconical chiral nematic liquid crystal phase of an achiral rigid bent-core mesogen. *Phys. Rev. E Stat. Nonlinear Biol. Soft Matter Phys.* **2014**, *89*, 022506. [[CrossRef](#)] [[PubMed](#)]
55. Wang, Y.; Singh, G.; Agra-Kooijman, D.M.; Gao, M.; Bisoyi, H.K.; Xue, C.; Fisch, M.R.; Kumar, S.; Li, Q. Room temperature heliconical twist-bend nematic liquid crystal. *CrystEngComm* **2015**, *17*, 2778–2782. [[CrossRef](#)]
56. Sreenilayam, S.P.; Panov, V.P.; Vij, J.K.; Shanker, G. The N_{TB} phase in an achiral asymmetrical bent-core liquid crystal terminated with symmetric alkyl chains. *Liq. Cryst.* **2017**, *44*, 244–253. [[CrossRef](#)]
57. Mandle, R.J. A Ten-Year Perspective on Twist-Bend Nematic Materials. *Molecules* **2022**, *27*, 2689. [[CrossRef](#)]
58. Mandle, R.J.; Archbold, C.T.; Sarju, J.P.; Andrews, J.L.; Goodby, J.W. The dependency of nematic and twist-bend mesophase formation on bend angle. *Sci. Rep.* **2016**, *6*, 36682. [[CrossRef](#)]
59. Mandle, R.J.; Goodby, J.W. Molecular flexibility and bend in semi-rigid liquid crystals: Implications for the heliconical nematic ground state. *Chem. Eur. J.* **2019**, *25*, 14454. [[CrossRef](#)]
60. Yu, G.; Wilson, M.R. All-atom simulations of bent liquid crystal dimers: The twist-bend nematic phase and insights into conformational chirality. *Soft Matter* **2022**, *18*, 3087–3096. [[CrossRef](#)]
61. Kumar, A. Dependency of the twist-bend nematic phase formation on the molecular shape of liquid crystal dimers: A view through the lens of DFT. *J. Mol. Liq.* **2022**, *354*, 118858. [[CrossRef](#)]
62. Arakawa, Y.; Komatsu, K.; Shiba, T.; Tsuji, H. Methylene-and thioether-linked cyanobiphenyl-based liquid crystal dimers CB_nSCB exhibiting room temperature twist-bend nematic phases and glasses. *Mater. Adv.* **2021**, *2*, 1760–1773. [[CrossRef](#)]
63. Archbold, C.T.; Davis, E.J.; Mandle, R.J.; Cowling, S.J.; Goodby, J.W. Chiral dopants and the twist-bend nematic phase—induction of novel mesomorphic behaviour in an apolar bimesogen. *Soft Matter* **2015**, *11*, 7547–7557. [[CrossRef](#)]
64. Dawood, A.A.; Gossel, M.C.; Luckhurst, G.R.; Richardson, R.M.; Timimi, B.A.; Wells, N.J.; Yousif, Y.Z. On the twist-bend nematic phase formed directly from the isotropic phase. *Liq. Cryst.* **2016**, *43*, 2–12. [[CrossRef](#)]

65. Dawood, A.A.; Gossel, M.C.; Luckhurst, G.R.; Richardson, R.M.; Timimi, B.A.; Wells, N.J.; Yousif, Y.Z. Twist-bend nematics, liquid crystal dimers, structure–property relations. *Liq. Cryst.* **2017**, *44*, 106–126.
66. Wang, D.; Liu, J.; Zhao, W.; Zeng, Y.; Huang, J.; Fang, J.; Chen, D. Facile Synthesis of Liquid Crystal Dimers Bridged with a Phosphonic Group. *Chem. Eur. J.* **2022**. [[CrossRef](#)]
67. Ramou, E.; Welch, C.; Hussey, J.; Ahmed, Z.; Karahaliou, P.K.; Mehl, G.H. The induction of the N_{tb} phase in mixtures. *Liq. Cryst.* **2018**, *45*, 1929–1935. [[CrossRef](#)]
68. Akdag, A.; Wahab, A.; Beran, P.; Rulisek, L.; Dron, P.I.; Ludvik, J.; Michl, J. Covalent Dimers of 1,3-Diphenylisobenzofuran for Singlet Fission: Synthesis and Electrochemistry. *J. Org. Chem.* **2015**, *80*, 80–89. [[CrossRef](#)]
69. Arakawa, Y.; Kang, S.; Tsuji, H.; Watanabe, J.; Konishi, G. Development of novel bistolane-based liquid crystalline molecules with an alkylsulfanyl group for highly birefringent materials. *RSC Adv.* **2016**, *6*, 16568–16574. [[CrossRef](#)]
70. Arakawa, Y.; Tsuji, H. Phase transitions and birefringence of bistolane-based nematic molecules with an alkyl, alkoxy and alkylthio group. *Mol. Cryst. Liq. Cryst.* **2017**, *647*, 422–429. [[CrossRef](#)]
71. Arakawa, Y.; Sasaki, Y.; Tsuji, H. Supramolecular hydrogen-bonded liquid crystals based on 4-*n*-alkylthiobenzoic acids and 4, 4'-bipyridine: Their mesomorphic behavior with comparative study including alkyl and alkoxy counterparts. *J. Mol. Liq.* **2019**, *280*, 153–159. [[CrossRef](#)]
72. Emerson, A.P.J.; Luckhurst, G.R. On the relative propensities of ether and methylene linkages for liquid crystal formation in calamitics. *Liq. Cryst.* **1991**, *10*, 861–868. [[CrossRef](#)]
73. Tasaka, T.; Okamoto, H.; Petrov, V.F.; Takenaka, S. Liquid crystalline properties of dissymmetric molecules part 5: The effects of alkyl chain length and linkages on thermal properties of smectic A and C phases in three aromatic ring systems. *Mol. Cryst. Liq. Cryst.* **2001**, *357*, 67–84. [[CrossRef](#)]
74. Balema, T.A.; Ulumuddin, N.; Murphy, C.J.; Slough, D.P.; Smith, Z.C.; Hannagan, R.T.; Wasio, N.A.; Larson, A.M.; Patel, D.A.; Groden, K.; et al. Controlling molecular switching via chemical functionality: Ethyl vs methoxy rotors. *J. Phys. Chem. C* **2019**, *123*, 23738–23746. [[CrossRef](#)]
75. McCurdy, R.M.; Prager, J.H. Thiaalkyl polyacrylates: The influence of sulfur in the side chain. *J. Polym. Sci. Part A Gen. Pap.* **1964**, *2*, 1185–1192. [[CrossRef](#)]